LAWRENCE
LIVERMORE
NATIONAL
LABORATORY

UCRL-JRNL-225356

Integrated Laser-Target Interaction Experiments on the RAL Petawatt Laser

P. K. Patel, M. H. Key, A. J. Mackinnon, R. Berry, M. Borghesi, D. M. Chambers, H. Chen, R. Clarke, C. Damian, R. Eagleton, R. Freeman, S. Glenzer, G. Gregori, R. Heathcote, D. Hey, N. Izumi, S. Kar, J. King, A. Nikroo, A. Niles, H. S. Park, J. Pasley, N. Patel, R. Shepherd, R. A. Snavely, D. Steinman, C. Stoeckl, M. Storm, R. Town, R. Van Maren, W. Theobald, S. C. Wilks, B. Zhang

October 17, 2006

Plasma Physics and Controlled Fusion

Disclaimer

Integrated Laser-Target Interaction Experiments on the RAL Petawatt Laser

P K Patel[1], M H Key[1], A J Mackinnon[1], R Berry[1], M Borghesi[7], D M Chambers[6], H Chen[1], R C Clarke[8], C Damian[1], R Heathcote[8], D Hey, R Eagleton[6], R R Freeman[5], S Glenzer[1], G Gregori[1], D Hey[5], N Izumi[1], S Kar[7], J A King[2], A Nikroo[3], A Niles[1], H-S Park[1], J Pasley[9], N Patel[5], R S Shepherd[1], R A Snavely[1], D Steinman[3], C Stoeckl[4], M Storm[4], R Town[1], R Van Maren[1], W Theobald[4], S C Wilks[1] and B Zhang[2]

[1] Lawrence Livermore National Laboratory, Livermore, CA 94550, USA
[2] Dept. of Applied Sciences, University of California, Davis, CA 95616, USA
[3] General Atomics, PO Box 85608, San Diego, CA 92186, USA
[4] Laboratory for Laser Energetics, University of Rochester, Rochester, NY 14623, USA
[5] Ohio State University, Columbus, OH 43210, USA
[6] Atomic Weapons Establishment, Aldermaston, Reading, RG7 4PR, UK
[7] Dept. of Physics, Queen's University of Belfast, Belfast, BY7 1NN, UK
[8] CCLRC Rutherford Appleton Laboratory, Didcot, OX11 0QX, UK
[9] University of California, San Diego, CA 92093, USA

1. Introduction

Since the construction of the first Petawatt laser on the Nova laser facility at Lawrence Livermore National Laboratory we are witnessing the emergence of similar Petawatt-class laser systems at laboratories all around the world [i]. This new generation of lasers, able to deliver several hundred joules of energy in a sub-picosecond pulse, has enabled a host of new discoveries to be made and continues to provide a valuable tool to explore new regimes in relativistic laser-plasma physics—encompassing high energy X-rays and -rays, relativistic electrons, intense ion beams, and superstrong magnetic fields [ii,iii,iv]. The coupling in the near-future of multi-kiloJoule Petawatt-class lasers with large-scale fusion lasers—including the NIF and Omega EP (US), LIL (France), and FIREX (Japan)—will further expand opportunities in fast ignition, high energy X-ray radiography, and high energy density physics research.

The 500 J Petawatt laser at the Rutherford Appleton Laboratory is currently the highest energy short-pulse laser in the world [v]. In this paper we describe a recent experimental campaign carried out on the facility. The campaign, performed by a large collaborative team from eight different laboratories, was designed to study a variety of relativistic laser-interaction phenomena including laser absorption, fast electron transport, proton heating, and high-brightness x-ray generation. The wide scope of the experiment necessitated the deployment of a very large set of diagnostics—in total twenty-five separate instruments. In order to obtain the most comprehensive set of measurements all twenty-five diagnostics were fielded simultaneously on every shot.

2. Experiment

The Vulcan Nd:glass Petawatt laser delivers over 400 J of energy onto target in a 400 fs FWHM (full-width at half-maximum) temporal pulse. It combines an OPCPA (optical parametric chirped-pulse amplification) front end with a mixed glass amplification chain. The amplified chirped pulse is recompressed by a pair of 94 cm diameter gold gratings to a 400 fs pulsewidth before delivery to the interaction chamber, where a 65 cm diameter f/3 off-axis parabola focuses it onto target. In this experiment the laser was incident with p-polarization at an angle of 28˚ to the target normal.

An extensive array of diagnostics—some twenty-five instruments in total—were fielded in and around the target chamber. The front side diagnostics included a single-hit CCD for measuring K-alpha yields, an Al K-shell X-ray spectrometer, an optical spectrometer measuring the specular reflected light, a neutron scintillator detector, an X-ray pinhole camera, and an X-ray diode array. The rear side diagnostics included two monochromatic XUV imagers operating at 68 eV and 256 eV, an XUV streak camera imaging at 68 eV, an optical imaging streak camera, a multi-layer hard X-ray spectrometer, a HOPG (highly oriented pyrolitic graphite) crystal X-ray spectrometer, a second single-hit K-alpha CCD camera, radiochromic film, and an MeV electron spectrometer. The requirement for all of the diagnostics to function simultaneously on each shot introduced considerable complexity to the experimental setup. To facilitate the design a 3-D CAD model was created of the entire target chamber, as well as each instrument. This enabled a single design to be reached which optimised the locations and viewing angles of each diagnostic whilst ensuring that no interferences would exist.

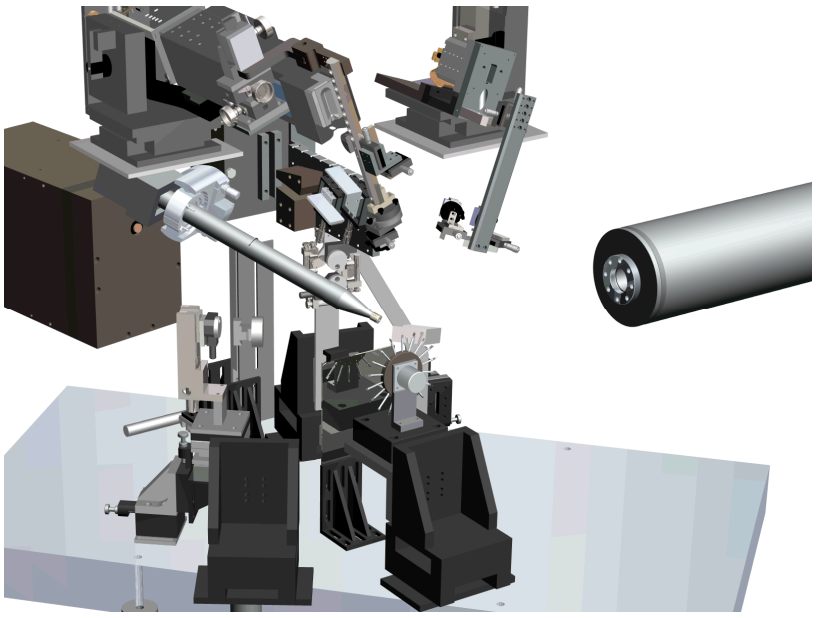

Fig. 1. Schematic of experimental setup inside the interaction chamber, highlighting a selection of the total diagnostic suite. The majority of these diagnostics are positioned to view the rear surface of the target.

3. Focal Spot

The laser focal spot was measured at low energy using a 40x microscope objective and 16-bit vacuum CCD directly imaging the focus of the parabola. The focal intensity distribution is an important parameter for 2-D or 3-D particle-in-cell (PIC) modeling of the laser-target interaction, particularly when one is interested in the spatial and directional characteristics of the fast electrons and their subsequent role in isochoric target heating, K-alpha x-ray production, and proton acceleration.

Figure 2 shows an image of the laser at best focus. The focal spot has a 6.9 µm FWHM. Approximately 20% of the incident laser energy is contained within this diameter. Given 400 J of energy on target this yields a peak intensity of $5x10^{20}$ W/cm^2. Half of the incident laser energy is contained within a 16 µm diameter spot.

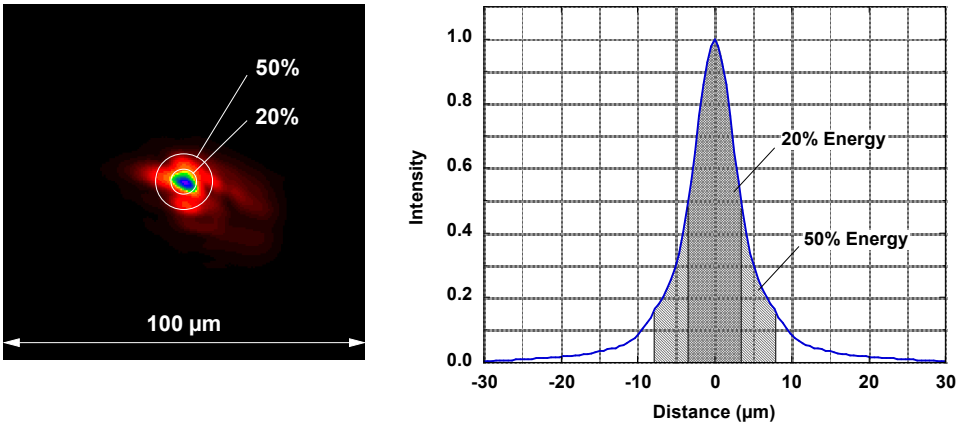

Fig. 2. Image of vacuum focal spot at low energy taken with a 16-bit CCD camera (left). Radial lineout of focal spot intensity showing 20% and 50% encircled energy boundaries (right).

4. Laser Absorption and Electron Heating

The very small interaction volume produced by a tightly focused beam inherently produces a non-1D interaction. The sharply varying radial intensity profile of the incident laser beam result in strong lateral gradients that will influence lateral thermal energy transport, both radiatively and collisionally, and lateral particle transport in the form of non-thermal or hot electrons. Figure 3 illustrates two of the diagnostics we have employed to study 2D lateral effects. The first is a time-integrated XUV imaging system consisting of a spherical mirror with a reflective multi-layer dielectric coating centered at 68 eV. The spherical mirror is used to image the rear surface of the target, via a second flat dielectric coated mirror, onto a 16-bit back-illuminated CCD camera. The second is a spherically bent crystal X-ray imager with a Bragg angle corresponding to the K-alpha line of Cu at 8.05 keV [vi]. X-rays from the target at this energy are imaged onto another 16-bit back-illuminated CCD camera.

The images in Fig. 3 are taken from a 400 J pulse tightly focused on the centre of a 330 µm square, 7 µm thick multi-layer target (5 µm Cu coated on both sides with 1 µm Al). The XUV image on the left shows the radiative emission at 68 eV from the rear surface of the foil. To first order the intensity of emission is a function of the temperature of the foil (for a perfect blackbody the radiative intensity would be

described by a Planckian thermal distribution). The foil is optically thick to 68 eV radiation; therefore the signal in the image predominantly reflects emission from the rear surface plasma. Whilst there is a small localised intense region at the centre of the foil it is interesting to note that the rest of the foil is relatively uniformly heated. The edges of the foil are relatively sharp indicating that the emission occurs early in time before significant hydrodynamic expansion takes place. This is true except for the plume extending to the right of the target. This plume may be from the front side plasma extending beyond the target or from late-time expansion of the central hotspot at the rear surface.

The right-hand image in Fig. 3 shows the corresponding data from the 8.05 keV X-ray imager. This image shows the 2-D spatial distribution of the Cu K-alpha X-ray emission. The diagnostic views the target in the horizontal plane, but at an angle of 54˚ to the target normal, thus explaining the foreshortening of the foil in the horizontal direction. The target is optically thin to these X-rays so they are able to come from the entire 5 μm thickness of Cu. Again we observe a small hotspot within an otherwise very uniformly emitting foil. This would indicate that the hot electrons generating the K-alpha X-rays may rapidly settle to a uniform spatial distribution over this size of foil (aside from the central intense spot).

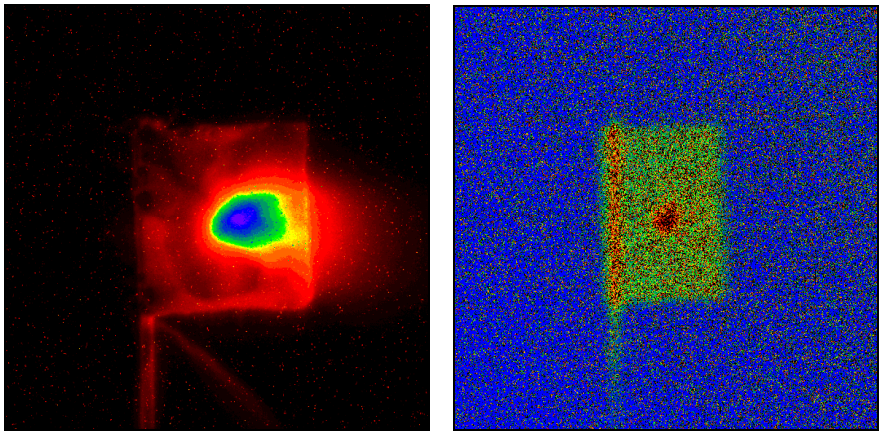

Fig. 3. Image of 68 eV XUV emission from the rear of a 330 μm square, 7 μm thick Al/Cu/Al target irradiated with 400 J laser pulse (left); corresponding Cu K-alpha emission at 8.05 keV recorded on the same shot (right).

X-ray spectral measurements were also obtained on these shots in the 8.0-8.2 keV region using a time-integrated X-ray crystal (HOPG) spectrometer. In these spectra X-rays are observed at shorter wavelengths than the cold K-alpha line. The X-rays correspond to transitions made in multiply-ionised Cu atoms where the stripping of outer valence electrons leads to a small increase in the energy gap between the n=1 and n=2 levels. The resulting shift in wavelength of the K-alpha line is thus correlated to the ionisation state of the material and can be used as a diagnostic of the mean ionisation and temperature. These data are reported in Gregori *et al.* [vii], wherein the authors infer temeratures on the order of 200 eV reached in the solid density tamped Copper.

5. Proton Generation

In a thin foil target the relativistic electrons driven into the target emerge at the rear surface and through charge separation create an extremely high strength electric field normal to the target surface. This field is capable of ionising atoms at the rear surface and accelerating them to a significant fraction of the speed of

light, on the order of a picosecond in time. The presence of hydrogen on the target surface, in the form of hydrocarbons, results in the preferential acceleration of protons (bare hydrogen nuclei) as the lightest ion present. The proton beams have some remarkable properties, including laser-to-proton energy conversion efficiencies of several percent, peak proton energies exceeding 50 MeV, and a high degree of directionality with very low transverse emittance [viii,ix,x].

In this experiment the proton beam was characterised using a multi-layer stack of radiochromic film (RCF) placed behind the target along the axis defined by the target normal. Each layer of RCF measures the radiation dose, or energy deposited within it by the beam of protons. Protons with higher energy travel through more layers before losing all their energy; thus, by measuring the deposited energy in each successive RCF layer in the stack one can reconstruct the energy spectrum of the proton beam.

Figure 4 shows the proton energy spectrum recorded from a 20 μm thick Cu foil irradiated with a 400 J pulse. For this shot the laser spot was defocused by moving the target 200 μm out of the plane of best focus. Whilst reducing the intensity on target this has been found to produce a more spatially uniform proton beam. The solid line in Fig. 4 is a best fit using an exponential energy distribution with a temperature kT=3.0 MeV and a total proton number of 7E13. The lowest energy data point is at 7.8 MeV. At lower energies the energy spectrum may not of course necessarily follow this fit and thus the total proton number is uncertain. Above 7.8 MeV however one can infer from the plot a total of 8.6 J of energy in the proton beam, equivalent to a laser-to-proton conversion efficiency of just over 2%.

In addition to the energy spectrum we also characterised the spatial characteristics of the beam at the source. This was done by using a 20 μm thick Cu foil pre-fabricated with a linear groove structure machined on the rear surface. The grooves have a separation of 3 μm and their pattern becomes superimposed on the spatial profile of the proton beam during the rapid initial acceleration period. This technique has been used previously to successfully characterise aspects of the spatial distribution of the electrons and protons during the acceleration process [xi].

Figure 5 shows a layer of radiochromic film corresponding to a mean proton energy of 15 MeV. The linear pattern of the grooves, oriented at 45°, can clearly be seen in the spatial profile of the proton beam. The outer edge of the proton beam spans 117 grooves. With a 3 μm groove separation this implies that the protons originate from a sources size of 350 μm diameter at the target surface. The FWHM of the beam spans 69 grooves, corresponding to a 206 μm diameter. The source size is actually a function of the proton energy; thus the source emitting area will be larger for proton energies below 15 MeV, and smaller for higher energies.

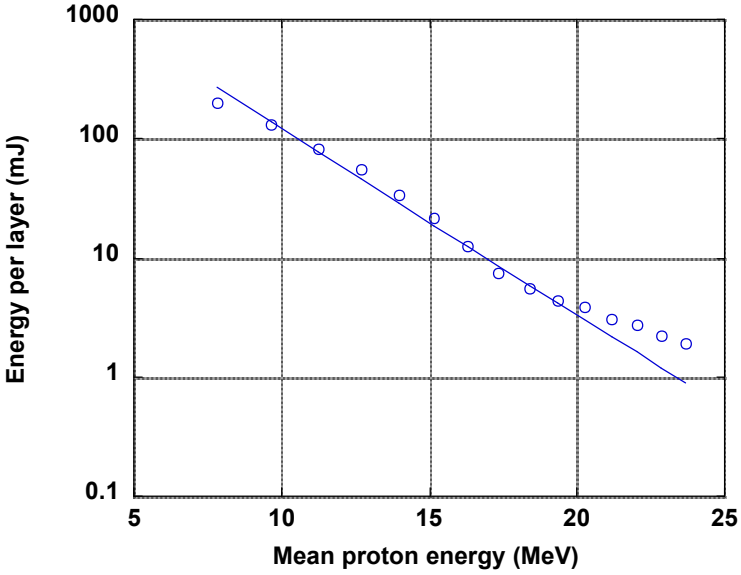

Fig. 4. Proton energy spectrum recorded on RCF for a 400 J pulse incident on a 20 μm thick Cu foil (circles). Solid line is a fit to the data calculated using 7E13 protons in an exponential energy distribution with kT=3.0 MeV.

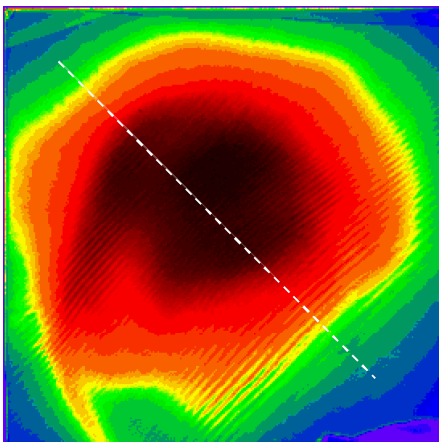

Fig. 5. Image of proton beam from 10th layer of radiochromic film, corresponding to a mean proton energy of 15 MeV. The 45˚ linear pattern seen in the beam corresponds to the groove pattern machined into the rear surface of the target foil.

6. Proton Heating

Recent experiments have demonstrated that laser-generated proton beams are sufficiently intense to isochorically heat other materials to 10's eV temperatures on impact [xii,xiii]. Proton heating provides a new method for very rapid heating of solid density materials (picosecond timescales). Since multi-MeV

protons have ranges of 10's to 100's of microns they deposit their energy fairly uniformly over that distance (until near the end of the range where the rate of energy deposition increases in the form of a Bragg peak). These properties sugges that proton heating could prove to be a useful tool for creating relatively uniform high energy density plasmas for quantitative study.

We investigated two geometries for proton heating this experiment: planar and focusing geometries. In the planar case the proton beam was produced from a 20 μm thick Cu foil under the same conditions described in Section 5. A second 10 μm thick Al foil was placed 200 μm behind the first foil along the target normal. In the focusing geometry the 20 μm thick Cu foil was shaped in the form of a hemisphere with a 1 mm diameter. A second foil (a multilayer CH/Al/CH foil of 14 μm total thickness) was placed close to the focus of the hemisphere. The laser is incident on the outer surface of the hemisphere. Figure 6 shows the 68 eV XUV emission imaged from the rear of the secondary foils for these two shots.

One sees that the heated region in the focusing geometry is substantially smaller, and slightly more intense (the peak counts are approximately 50% higher). The heated region in the planar case has a FWHM diameter of 280 μm. This corresponds closely to the measured source size of the proton beam. In the focusing case the diameter of the heated region is only 94 μm FHWM indicating that the proton beam undergoes a degree of focusing or collimation. Based on an absolute calibration of the instrument the observed signal indicates that thermal temperatures on the order of 100 eV or more are reached. An accurate figure for the temperature however depends on detailed modeling ot the hydrodynamic expansion of the plasma, taking into proper account time-dependence and opacity effects on the emitted radiative intensity. Such modeling is currently being performed and will provide more quantitative information on the the plasma conditions reached in the proton-heated foils.

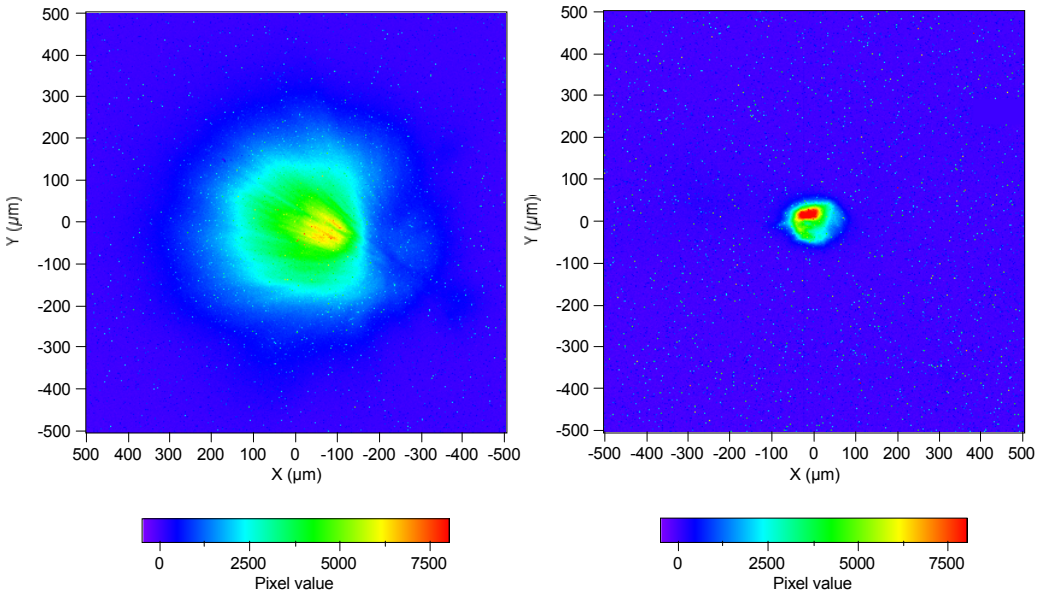

Fig. 6. 68 eV XUV emission from the rear of proton-heated foils in (a) planar and (b) focusing geometries. Data are plotted on the same colour scale to facilitate direct comparison of observed emission intensity.

7. Conclusion

In this paper we give a brief overview of a large collaborative experimental campaign carried out on the Rutherford Appleton Laboratory 500 J Petawatt laser. An extensive suite of diagnostics was employed to enable as comprehensive a set of measurements as possible of the X-ray, XUV, optical, electron, proton, and neutron emission from the plasma created by the irradiation of a solid target by a high intensity sub-picosecond laser pulse. This method of experimentally characterising the plasma through multiple and varied channels on a single shot may provide a useful means for benchmarking the increasingly sophisticated laser-plasma interaction codes being developed for the relativistic regime.

Acknowledgements

The authors wish to thank the staff of the Central Laser Facility, CCLRC Rutherford Appleton Laboratory. This work was performed under the auspices of the U.S. Department of Energy by the University of California, Lawrence Livermore National Laboratory, under contract W-7405-ENG-48.

References

[1] Perry MD et al., Opt. Lett. **24,** 160 (1999)
[ii] Hatchett SP et al., Phys. Plasmas, **7,** 2076 (2000)
[iii] Krushelnik K et al., Phys. Plasmas **7,** 2055 (2000)
[iv] Norreys PA et al., Plasma Phys. Control. Fusion **46,** B13 (2004)
[v] Danson, C et al. IAEA J. Nucl. Fusion (in press)
[vi] Koch JA et al., Rev. Sci. Instr. **74,** 2130 (2003)
[vii] Gregori G et al., Contrib. Plasma Phys. **45,** No. 3-4, 284-292 (2005)
[viii] Clark, EL et al. Phys. Rev. Lett. **84,** 670 (2000)
[ix] Snavely RA et al., Phys. Rev. Lett. **85,** 2945 (2000)
[x] Mackinnon AJ et al., Phys. Rev. Lett. **88,** 215006 (2002)
[xi] Cowan TE et al., Phys. Rev. Lett. (2004)
[xii] Patel PK et al., Phys. Rev. Lett. **92,** 125004 (2003)
[xiii] Snavely RA et al., Proc. 3rd International IFSA Conference, Monterey, CA (2003)